International Journal of Heat and Mass Transfer 52 (2009) 588–596

Contents lists available at ScienceDirect

International Journal of Heat and Mass Transfer

journal homepage: www.elsevier.com/locate/ijhmt

Laminar and turbulent free convection in a composite enclosure

Edimilson J. Braga, Marcelo J.S. de Lemos *

Departamento de Energia – IEME, Instituto Tecnológico de Aeronáutica – ITA, 12228-900 São José dos Campos, SP, Brazil

ARTICLE INFO

Article history:
Received 9 April 2008
Received in revised form 2 July 2008
Available online 31 August 2008

Keywords:
Porous media
Heat transfer
Natural convection
Turbulence modeling

ABSTRACT

Turbulent natural convection in a two-dimensional horizontal composite square cavity, isothermally heated at the left side and cooled from the opposing surface, is numerically analyzed using the finite volume method. The composite square cavity is formed by three distinct regions, namely, clear, porous and solid region. The development of a numerical tool able to treat all these regions as one computational domain is of advantage for engineering design and analysis of passive thermal control systems. Governing equations are written in terms of primitive variables and are recast into a general form. It was found that the fluid begins to permeate the porous medium for values of *Ra* greater than 10^6. Nusselt number values show that for the range of *Ra* analyzed there is no significant variation between the laminar and turbulent model solution. When comparing the effects of *Ra*, k_s/k_f and *Da* on *Nu*, results indicate that the solid phase properties have a greater influence in enhancing the overall heat transferred trough the cavity.

1. Introduction

Buoyancy-driven flows in porous enclosures have been extensively studied recently due to their many engineering and environmental applications. Underground spread of pollutants, environmental control, grain storage, food and material processing, geothermal systems, oil extraction, storage of nuclear waste material, solar power collectors, optimal design of furnaces, nuclear reactor safety, compact heat exchangers, packed-bed catalytic reactors and passive thermal control devices are some examples of applications of heat removal or addition by free convection mechanism.

Studies concerning natural convection in porous media can be found in the monographs of [1,2]. The case of free convection in a rectangular cavity heated on one side and cooled at the opposing side is also an important problem in thermal convection in porous media. The works of [3–8] have further contributed with some classical results to this problem. Reference [9] considered a numerical study of the steady free convection flow in rectangular and oblique cavities filled with homogeneous porous media using a nonlinear axis transformation. The Darcy momentum and energy equations were solved numerically using the (ADI) method. According to Massarotti et al. [10], many researchers ignored transient effects although for certain porous media flows transient analysis is required. For such cases, the velocity correction method can be based on a time stepping scheme. Also, implementation of different numerical techniques such as semi-implicit [11,12] quasi-implicit [13] and fully implicit schemes are possible. Other important contributions on free convection in porous media are available in the literature published in the last few decades [14–21], which are here referred to for the sake of completeness and for conveying to the reader a broader view of the subject here studied. However, most works found in the literature are restricted to cavities consisting of a single domain, either an unobstructed space or an enclosure filled with a fluid saturated porous medium, covering both laminar and turbulent flow regimes.

Turbulence modeling is necessary when time fluctuations of the flow properties are also considered, in addition to spatial deviations. For such analyses, there are two possible methodologies to follow in order to obtain macroscopic equations. The first one applies the time-average operator followed by volume-averaging [22–25]. In the second path, volume-averaging is used of before time-averaging is considered [26–28]. However, both sets of macroscopic transport equations are equivalent when examined under the *double decomposition* concept [29,30], which has been also extended to non-buoyant heat transfer in porous media [31,32]. Further, a consistent and systematic study based on the *double-decomposition theory* for treating turbulent buoyant flows [33–37], mass transfer [38], non-equilibrium heat transfer [39,40], double diffusion [41] and transport across the interface between a porous medium and a clear region [42,43], has been published. However, none of these papers by de Lemos and coworkers [29–43] have tackle a problem similar to the one here investigate, which deals with a three-layer composite cavity configuration.

Motivated by the many engineering applications mentioned earlier, as well as the observed lack of turbulent flow solutions

* Corresponding author. Tel.: +55 12 3947 5860; fax: +55 12 3947 5842.
E-mail address: delemos@ita.br (M.J.S. de Lemos).

0017-9310/$ - see front matter © 2008 Elsevier Ltd. All rights reserved.
doi:10.1016/j.ijheatmasstransfer.2008.07.012

Nomenclature

Latin characters

c_F	Forchheimer coefficient
$c_{1,2,3,k,\mu}$	model constants
c_p	fluid specific heat
Da	Darcy number, K/H^2
D_p	particle diameter used in computing the permeability K
$\mathbf{g}$	gravity acceleration vector
H	cavity height
K	permeability, $K = \frac{D_p^2\phi^3}{144(1-\phi)^2}$
k	turbulent kinetic energy
k_f	fluid thermal conductivity
k_s	solid thermal conductivity
Nu	$Nu = hH/k$, Nusselt number
Ra	$Ra = \frac{g\beta H^3\Delta T}{\nu\alpha}$, Rayleigh number
T	non-dimensional temperature, $\frac{\langle\overline{T}\rangle^i - T_C}{T_H - T_C}$
$\mathbf{u}$	microscopic velocity
$\mathbf{u}_D$	Darcy or superficial velocity (volume average of $\mathbf{u}$)
x, y	cartesian coordinates

Greek characters

α	fluid thermal diffusivity
β	fluid thermal expansion coefficient
β_i	jump coefficient at interface clear-porous media
ΔV	representative elementary volume
ΔV_f	fluid volume inside ΔV
ε	dissipation rate of k
μ	fluid dynamic viscosity
μ_{t_ϕ}	macroscopic turbulent viscosity
ν	fluid kinematic viscosity
ρ	fluid density
$\sigma_{k,\varepsilon,T}$	turbulence model constants
ϕ	$\phi = \Delta V_f/\Delta V$, porosity

Special characters

φ	general variable
$\bar{\varphi}$	temporal average
φ'	temporal fluctuation
$\langle\varphi\rangle^i$	intrinsic average
$\langle\varphi\rangle^v$	volume average
${}^i\varphi$	spatial deviation
$\boldsymbol{\varphi}$	vectorial general variable
φ_{eff}	effective value, $\varphi_{eff} = \phi\varphi_f + (1-\phi)\varphi_s$
$\varphi_{s,f}$	solid/fluid
$\varphi_{H,C}$	hot/cold
$(\,)^T$	transpose
φ_ϕ	macroscopic value

for compound cavity flows, which may contain solid material and free spaces in addition to internal porous layers, this paper presents results for turbulent flows in a composite heated enclosure. As the overall heat flux across the cavity is from left to right, this geometry is here considered a horizontal cavity. Further, the enclosure is formed by three distinct regions, namely, a clear, a porous and a solid region. The turbulence model here adopted is the standard k–ε with wall function.

It is expected that the present contribution can benefit engineering design and analysis of passive thermal control systems, for example.

2. Geometry under analysis

The problem considered is shown schematically in Fig. 1a, and refers to the two-dimensional flow of a Boussinesq fluid of Prandtl number, $Pr = 1$, in a square cavity of side $H = 1$ m. The cavity is assumed to be of infinite depth along the z-axis and is isothermally heated from the left side and cooled from the opposing side. Heat flows horizontally and for this reason the nomenclature "horizontal cavity" is here assumed. Further, the cavity is equally divided in three distinct regions, namely, clear, porous and solid region.

The no-slip condition is applied for velocity and the resulting flow is treated as steady. The controlling parameter is the Rayleigh number, $Ra = \frac{g\beta H^3\Delta T}{\nu\alpha}$. Further, a relationship for the permeability was proposed in [44] for circular rods, which are in good accord with the empirical expression proposed by [45], as

$$K = \frac{D_p^2\phi^3}{144(1-\phi)^2} \tag{1}$$

where D_p is the equivalent diameter of the particle composing the porous medium.

3. Governing equations

The equations used herein are derived in details in the work of [33–37], and for this reason they will be just reproduced here. Basically, for porous media analysis, a macroscopic form of the governing equations is obtained by taking the volumetric average of the entire equation set. In that development, the porous medium is considered to be rigid and saturated by an incompressible fluid.

The macroscopic continuity equation is given by

$$\nabla\cdot\bar{\mathbf{u}}_D = 0 \tag{2}$$

The Dupuit–Forchheimer relationship, $\bar{\mathbf{u}}_D = \phi\langle\bar{\mathbf{u}}\rangle^i$, has been used and $\langle\bar{\mathbf{u}}\rangle^i$ identifies the intrinsic (liquid) average of the local velocity vector $\bar{\mathbf{u}}$. The macroscopic time-mean Navier–Stokes (NS) equation for an incompressible fluid with constant properties is given as

$$\rho\left[\frac{\partial\bar{\mathbf{u}}_D}{\partial t} + \nabla\cdot\left(\frac{\bar{\mathbf{u}}_D\bar{\mathbf{u}}_D}{\phi}\right)\right] = -\nabla\left(\phi\langle\bar{p}\rangle^i\right) + \mu\nabla^2\bar{\mathbf{u}}_D + \nabla\cdot\left(-\rho\phi\langle\overline{\mathbf{u}'\mathbf{u}'}\rangle^i\right) - \rho\beta_\phi\mathbf{g}\phi\left(\langle\overline{T}\rangle^i - T_{ref}\right) - \left[\frac{\mu\phi}{K}\bar{\mathbf{u}}_D + \frac{c_F\phi\rho|\bar{\mathbf{u}}_D|\bar{\mathbf{u}}_D}{\sqrt{K}}\right] \tag{3}$$

When treating turbulence with statistical tools, the correlation $-\rho\overline{\mathbf{u}'\mathbf{u}'}$ appears after application of the time-average operator to the local instantaneous NS equation. Applying further the volume average procedure to this correlation results in the term $-\rho\phi\langle\overline{\mathbf{u}'\mathbf{u}'}\rangle^i$. This term is here recalled the *Macroscopic Reynolds Stress Tensor* (MRST). Further, a model for the MRST in analogy with the Boussinesq concept for clear fluid can be written as

$$-\rho\phi\langle\overline{\mathbf{u}'\mathbf{u}'}\rangle^i = \mu_{t_\phi}2\langle\overline{\mathbf{D}}\rangle^v - \frac{2}{3}\phi\rho\langle k\rangle^i\mathbf{I} \tag{4}$$

where

$$\langle\overline{\mathbf{D}}\rangle^v = \frac{1}{2}\left[\nabla(\phi\langle\bar{\mathbf{u}}\rangle^i) + [\nabla(\phi\langle\bar{\mathbf{u}}\rangle^i)]^T\right] \tag{5}$$

is the macroscopic deformation rate tensor, $\langle k\rangle^i$ is the intrinsic average for k and μ_{t_ϕ} is the macroscopic turbulent viscosity. The macroscopic turbulent viscosity, μ_{t_ϕ}, is modeled similarly to the case of clear fluid flow and a proposal for it was presented in [30] as

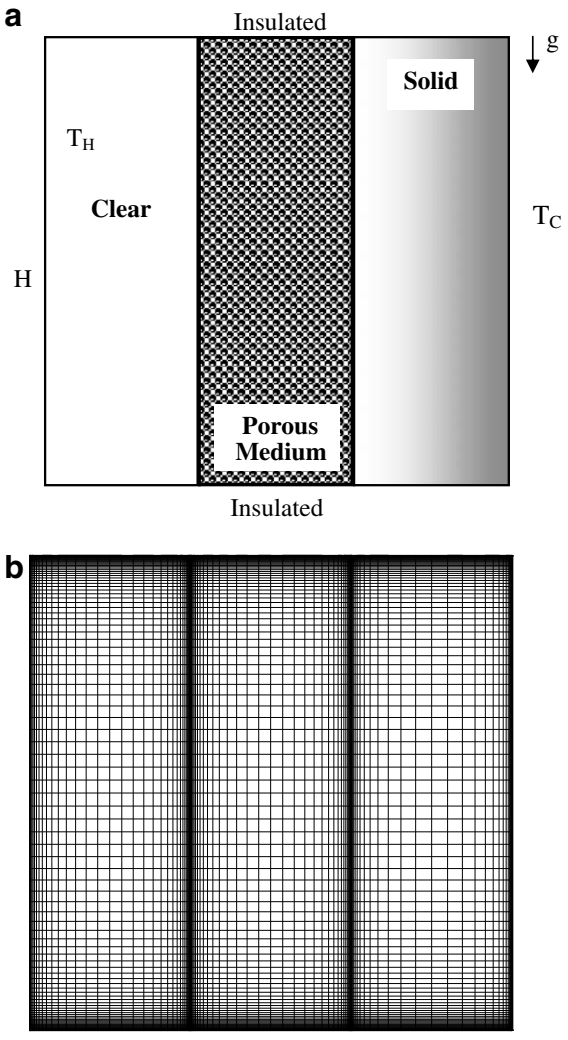

Fig. 1. Problem considered: (a) composite cavity, (b) grid used in all calculations: 112 × 112.

$$\mu_{t_\phi} = \rho c_\mu \frac{\langle k\rangle^{i\,2}}{\langle \varepsilon\rangle^{i}} \tag{6}$$

In a similar way, applying both time and volumetric average to the microscopic energy equation, for either the fluid or the porous matrix, two equations arise. Assuming further the *Local Thermal Equilibrium* (LTE) hypothesis, which considers $\langle\overline{T}_f\rangle^i = \langle\overline{T}_s\rangle^i = \langle\overline{T}\rangle^i$, and adding up these two equations, one has,

$$\begin{aligned}(\rho c_p)_f \nabla\cdot(\bar{\mathbf{u}}_D\langle\overline{T}\rangle^i) &= \nabla\cdot\{[k_f\phi + k_s(1-\phi)]\nabla\langle\overline{T}\rangle^i\} \\ &\quad + \nabla\cdot\left[\frac{1}{\Delta V}\int_{A_i}\mathbf{n}(k_f\overline{T}_f - k_s\overline{T}_s)\,dS\right] \\ &\quad - (\rho c_p)_f\nabla\cdot[\phi(\langle^i\bar{\mathbf{u}}^i\overline{T}_f\rangle^i)]\end{aligned} \tag{7}$$

A model for the transient form of Eq. (7) has been given in detail in [31,32], as,

$$\begin{aligned}&\{(\rho c_p)_f\phi + (\rho c_p)_s(1-\phi)\}\frac{\partial\langle\overline{T}\rangle^i}{\partial t} + (\rho c_p)_f\nabla\cdot(\mathbf{u}_D\langle\overline{T}\rangle^i) \\ &\quad = \nabla\cdot\{\mathbf{K}_{eff}\cdot\nabla\langle\overline{T}\rangle^i\}\end{aligned} \tag{8}$$

where, $\mathbf{K}_{eff}$, given by

$$\mathbf{K}_{eff} = [\phi k_f + (1-\phi)k_s]\mathbf{I} + \mathbf{K}_{tor} + \mathbf{K}_t + \mathbf{K}_{disp} + \mathbf{K}_{disp,t} \tag{9}$$

is the effective conductivity tensor. In order to be able to apply (8), it is necessary to determine the conductivity tensors in (9), i.e., $\mathbf{K}_{tor}$, $\mathbf{K}_t$, $\mathbf{K}_{disp}$ and $\mathbf{K}_{disp,t}$. Following [24], this can be accomplished for the *tortuosity* and *thermal dispersion* conductivity tensors, $\mathbf{K}_{tor}$ and $\mathbf{K}_{disp}$, by making use of a unit cell subjected to periodic boundary conditions for the flow and a linear temperature gradient imposed over the domain. The conductivity tensors are then obtained directly from the microscopic results for the unit cell [24].

4. Turbulence model

The turbulent heat flux and turbulent thermal dispersion terms appearing in (9), $\mathbf{K}_t$ and $\mathbf{K}_{disp,t}$, which cannot be determined from unit cell calculations [24], are modeled here through the eddy diffusivity concept, similarly to [25,30]. It should be noticed that these terms arise only if the flow is turbulent, whereas the tortuosity and the thermal dispersion terms exist for both laminar and turbulent flow regimes.

Starting out from the time averaged energy equation coupled with the microscopic modeling for the turbulent heat flux through the eddy diffusivity concept, one can write, after volume-averaging,

$$-(\rho c_p)_f\langle\overline{\mathbf{u}'T_f'}\rangle^i = (\rho c_p)_f\frac{\nu_{t_\phi}}{\sigma_T}\nabla\langle\overline{T}_f\rangle^i \tag{10}$$

where the symbol ν_{t_ϕ} expresses the macroscopic eddy viscosity, $\mu_{t_\phi} = \rho_f\nu_{t_\phi}$, given by (6) and σ_T is a constant. According to (10), the macroscopic heat flux due to turbulence is taken as the sum of the turbulent heat flux and the turbulent thermal dispersion [32]. Therefore, the sum of the components of the conductivity tensor $\mathbf{K}_t$ and $\mathbf{K}_{disp,t}$ can be expressed as

$$\mathbf{K}_t + \mathbf{K}_{disp,t} = \phi(\rho c_p)_f\frac{\nu_{t_\phi}}{\sigma_T}\mathbf{I} \tag{11}$$

Transport equations for $\langle k\rangle^i = \langle\overline{\mathbf{u}'\cdot\mathbf{u}'}\rangle^i/2$ and $\langle\varepsilon\rangle^i = \mu\langle\overline{\nabla\mathbf{u}'\cdot(\nabla\mathbf{u}')^T}\rangle^i/\rho$ in their so-called high Reynolds number form are proposed in [30] and extended in [34] to incorporate the buoyant effects as:

$$\begin{aligned}\rho\left[\frac{\partial}{\partial t}(\phi\langle k\rangle^i) + \nabla\cdot(\bar{\mathbf{u}}_D\langle k\rangle^i)\right] &= \nabla\cdot\left[\left(\mu + \frac{\mu_{t_\phi}}{\sigma_k}\right)\nabla(\phi\langle k\rangle^i)\right] \\ &\quad + P^i + G^i + G^i_\beta - \rho\phi\langle\varepsilon\rangle^i\end{aligned} \tag{12}$$

$$\begin{aligned}\rho\left[\frac{\partial}{\partial t}(\phi\langle\varepsilon\rangle^i) + \nabla\cdot(\bar{\mathbf{u}}_D\langle\varepsilon\rangle^i)\right] &= \nabla\cdot\left[\left(\mu + \frac{\mu_{t_\phi}}{\sigma_\varepsilon}\right)\nabla(\phi\langle\varepsilon\rangle^i)\right] \\ &\quad + c_1P^i\frac{\langle\varepsilon\rangle^i}{\langle k\rangle^i} + c_2\frac{\langle\varepsilon\rangle^i}{\langle k\rangle^i}G^i + c_1c_3G^i_\beta\frac{\langle\varepsilon\rangle^i}{\langle k\rangle^i} - c_2\rho\phi\frac{\langle\varepsilon\rangle^{i\,2}}{\langle k\rangle^i}\end{aligned} \tag{13}$$

Table 1
Cases investigated using turbulence model

ϕ	$Da = K/H^2$	k_s/k_f	Pr	Ra
Variation of Rayleigh number, Ra				
9.50E−01	2.382E−06	1.00E+00	1.00E+00	1.00E+04
9.50E−01	2.382E−06	1.00E+00	1.00E+00	1.00E+06
9.50E−01	2.382E−06	1.00E+00	1.00E+00	1.00E+08
9.50E−01	2.382E−06	1.00E+00	1.00E+00	1.00E+10
9.50E−01	2.382E−06	1.00E+00	1.00E+00	1.00E+12
Variation of thermal conductivity ratio, k_s/k_f				
9.50E−01	2.382E−06	1.00E+01	1.00E+00	1.00E+08
9.50E−01	2.382E−06	1.00E+02	1.00E+00	1.00E+08
Variation of Darcy number, $Da = K/H^2$				
9.50E−01	2.38E−04	1.00E+00	1.00E+00	1.00E+08
9.50E−01	2.38E−02	1.00E+00	1.00E+00	1.00E+08

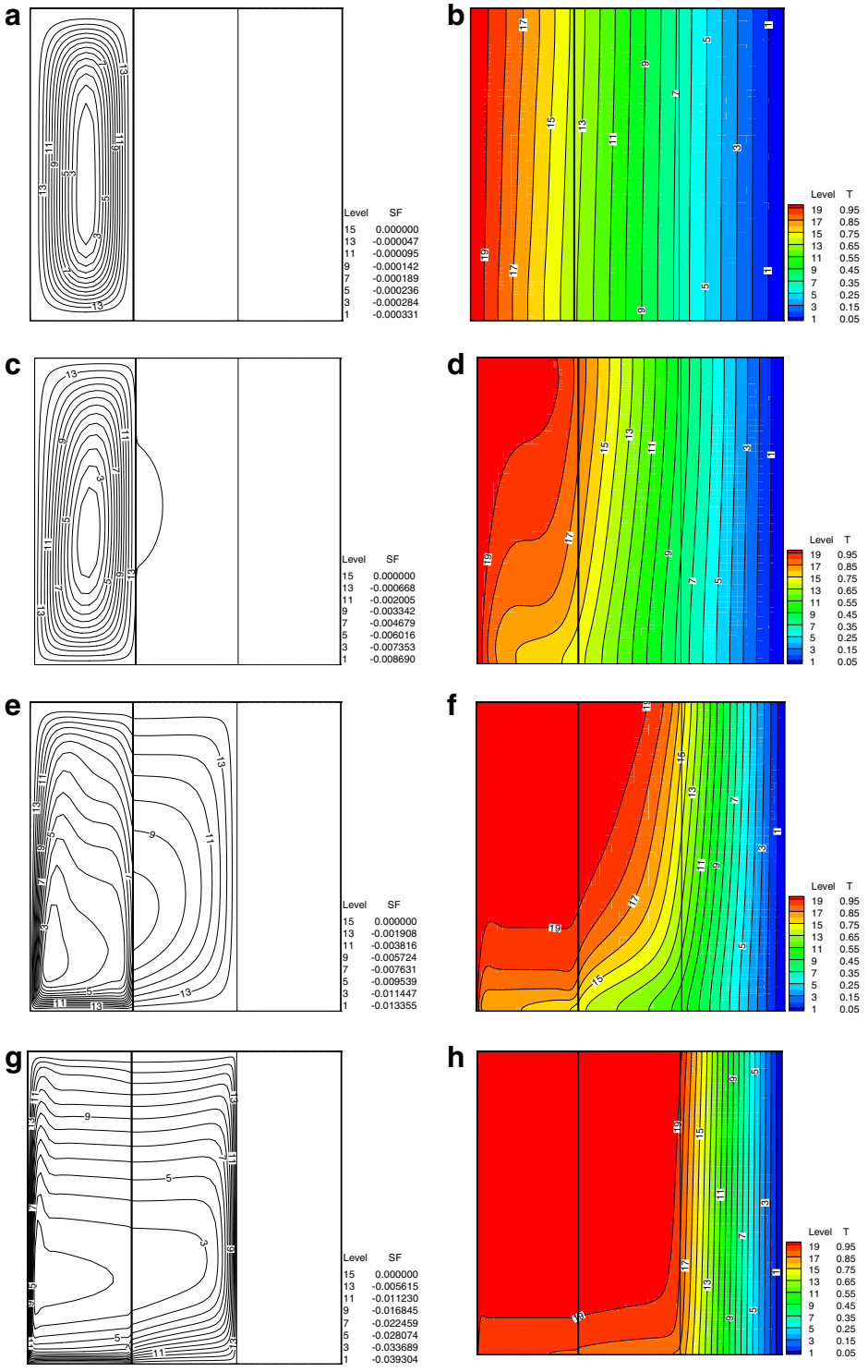

Fig. 2. Streamlines (left) and isotherms (right) for a composite cavity with $\phi = 0.95$, $Da = 0.2382 \times 10^{-5}$, $k_s/k_f = 1$ and $Pr = 1$: (a and b) $Ra = 10^4$, (c and d) $Ra = 10^6$, (e and f) $Ra = 10^6$, (g and h) $Ra = 10^{10}$.

where c_1, c_2, c_3 and c_k are constants, $P^i = -\rho\langle\overline{\mathbf{u}'\mathbf{u}'}\rangle^i : \nabla\bar{\mathbf{u}}_D$ is the production rate of $\langle k\rangle^i$ due to gradients of $\bar{\mathbf{u}}_D$, $G^i = c_k\rho\frac{\phi\langle k\rangle^i|\bar{\mathbf{u}}_D|}{\sqrt{K}}$ is the generation rate of the intrinsic average of k due to the action of the porous matrix and $G^i_\beta = \phi\frac{\mu_{t_\phi}}{\sigma_t}\mathbf{g}\beta_\phi\nabla\langle\overline{T}\rangle^i$ is the generation rate of $\langle k\rangle^i$ due to the buoyant effects.

Here, a word about the choice of a volume-averaged k–ε model to handle turbulence in hybrid (porous/clear) domains seems timely. It is the authors' believe that a macroscopic view of flow and heat transfer in such media can bring benefits to the design and analysis of flows occurring in the environment and in engineering equipment. Solving the intra-porous fine-flow structure would demand an enormous amount of computational resources, which is most of the time incompatible with the desirable reduction of costs in performing practical flow simulations. In addition, simulating turbulent flow and heat transfer in multi-domains (Fig. 1a), using only one set of equations, reduces the complexity of numerical analyses.

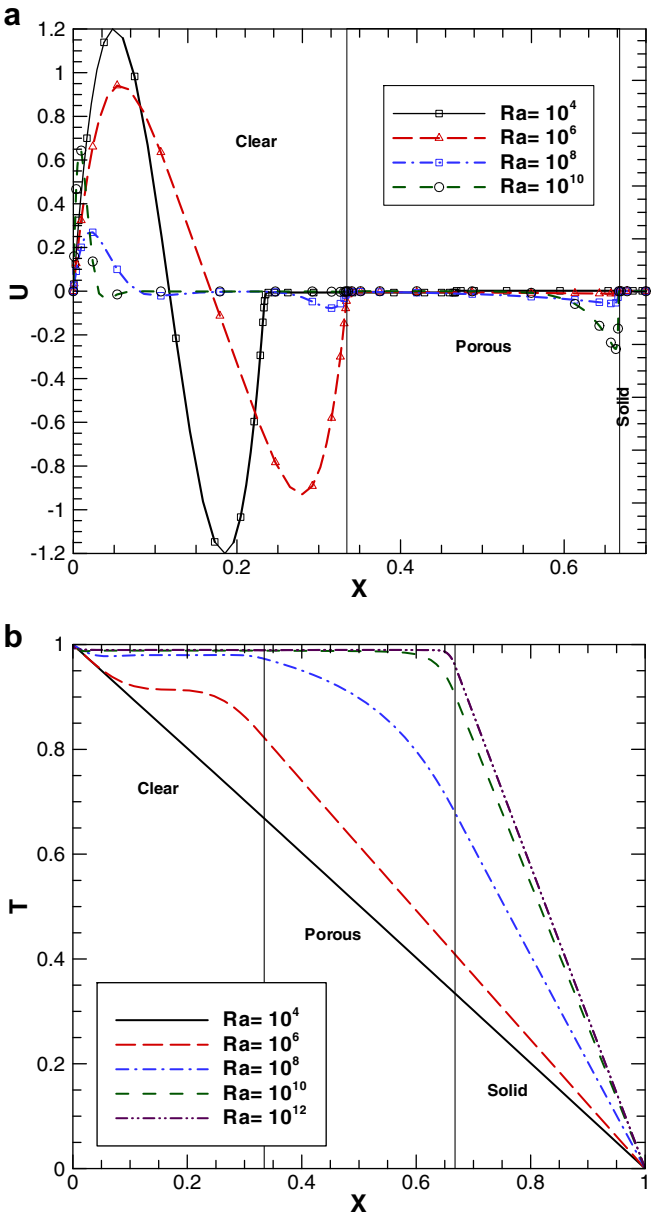

Fig. 3. Effect of *Ra* on vertical velocity (a) and temperature fields (b) at cavity mid-height $y = H/2$ for $\phi = 0.95$, $Da = 0.2382 \times 10^{-5}$, $k_s/k_f = 1$ and $Pr = 1$.

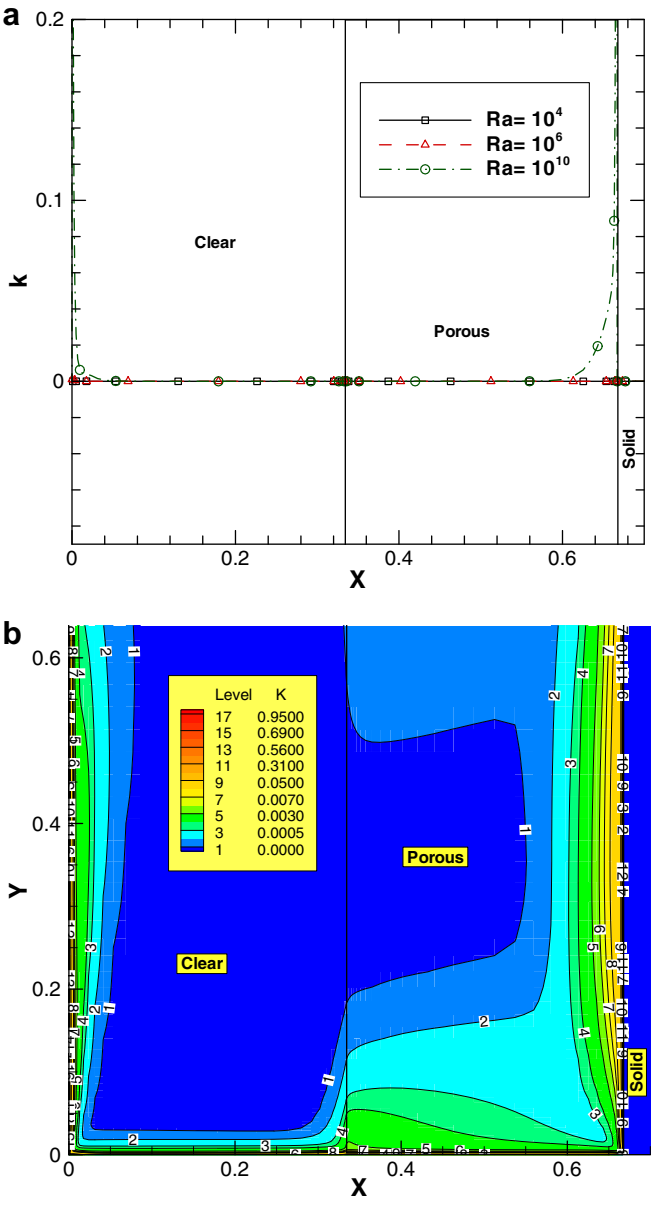

Fig. 4. Turbulent kinetic energy in a composite square cavity, $\phi = 0.95$, $Da = 0.2382 \times 10^{-5}$, $k_s/k_f = 1$ and $Pr = 1$: (a) effect of *Ra* at cavity mid-height, (b) color map and isolines for $Ra = 10^{10}$.

Accordingly, the macroscopic k–ε model developed earlier [29–43] brings a compromise between accuracy and economy, avoiding excessive computational time when resolving primitive variables such as the volumetric velocity, pressure and temperatures. In addition, the well-known shortcomings of the standard two-equation model, such as modest performance in recirculating flows, are counterbalanced by the fact that a linear stress–strain relationship, which is inherent to the k–ε model, enhances numerical stability besides being easy to program in existing code architectures.

5. Nusselt number

The local Nusselt number on the hot wall for the square cavity at $x = 0$ is defined as

$$Nu_y = hH/k \therefore Nu_y = \left(\frac{\partial \langle T \rangle^{v}}{\partial x}\right)_{x=0} \frac{H}{T_H - T_C} \tag{14}$$

and the average Nusselt number is given by

$$Nu = \frac{1}{H}\int_0^H Nu_y \, dy \tag{15}$$

6. Interface conditions

The interface conditions between the clear region and the porous medium follows the work of [46] using the shear stress jump concept. In Fig. 1 it was shown a hybrid domain where, for the interface clear-porous media, one has,

$$\bar{\mathbf{u}}_D|_{\phi<1} = \bar{\mathbf{u}}_D|_{\phi=1} \tag{16}$$

$$\langle \bar{p} \rangle^{i}|_{\phi<1} = \langle \bar{p} \rangle^{i}|_{\phi=1} \tag{17}$$

$$\phi^{-1}\frac{\partial \bar{u}_{D_1}}{\partial x_2}\bigg|_{\phi<1} - \frac{\partial \bar{u}_{D_1}}{\partial x_2}\bigg|_{\phi=1} = \frac{\beta_i}{\sqrt{K}}\bar{u}_{D_1}\bigg|_{\text{interface}} \tag{18}$$

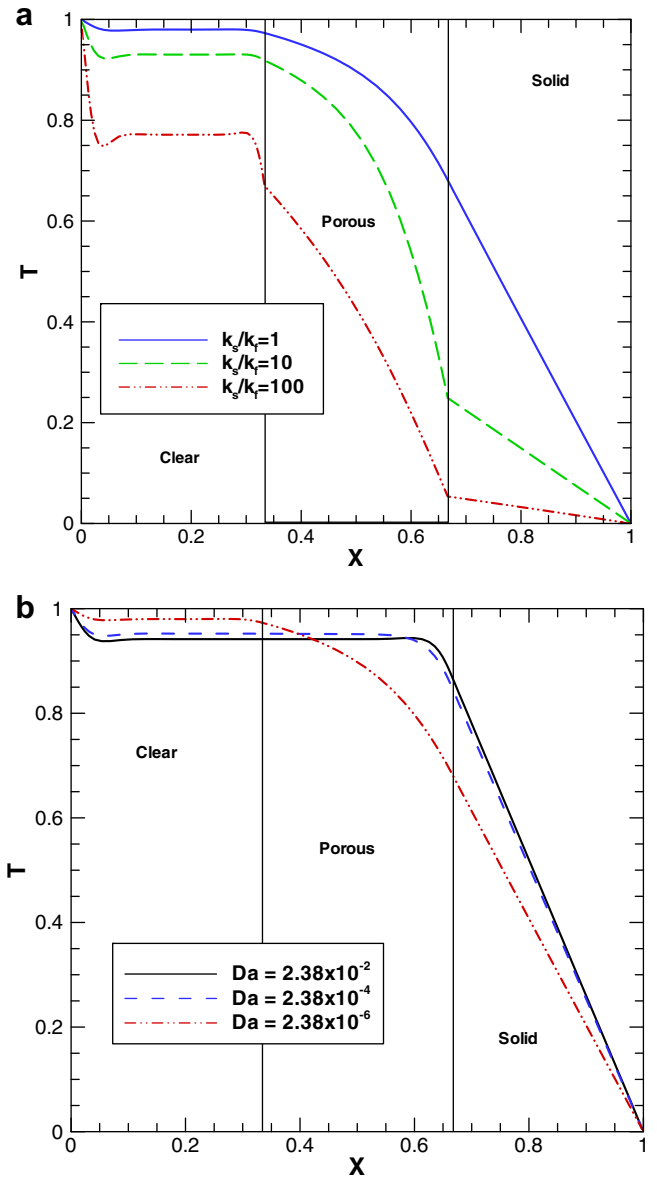

Fig. 5. Effect of thermal conductivity ratio k_s/k_f (a) and Darcy number $Da = K/H^2$ (b) on temperature distribution at cavity mid-height $y = H/2$ for $\phi = 0.95$, $Ra = 10^{-8}$ and $Pr = 1$.

$$\langle k\rangle^{v}|_{\phi<1} = \langle k\rangle^{v}|_{\phi=1} \tag{19}$$

$$\left(\mu + \frac{\mu_{t_\phi}}{\sigma_k}\right)\frac{\partial\langle k\rangle^{v}}{\partial x_2}\bigg|_{\phi<1} = \left(\mu + \frac{\mu_t}{\sigma_k}\right)\frac{\partial\langle k\rangle^{v}}{\partial x_2}\bigg|_{\phi=1} \tag{20}$$

$$\langle \varepsilon\rangle^{v}|_{\phi<1} = \langle \varepsilon\rangle^{v}|_{\phi=1} \tag{21}$$

$$\left(\mu + \frac{\mu_{t_\phi}}{\sigma_\varepsilon}\right)\frac{\partial\langle \varepsilon\rangle^{v}}{\partial x_2}\bigg|_{\phi<1} = \left(\mu + \frac{\mu_t}{\sigma_\varepsilon}\right)\frac{\partial\langle \varepsilon\rangle^{v}}{\partial x_2}\bigg|_{\phi=1} \tag{22}$$

$$\langle \overline{T}\rangle^{i}|_{\phi<1} = \langle \overline{T}\rangle^{i}|_{\phi=1} \tag{23}$$

$$\mathbf{e}_2 \cdot (\mathbf{K}_{\text{eff}} \cdot \nabla\langle \overline{T}\rangle^{i})|_{\phi<1} = k_f \frac{\partial\langle \overline{T}\rangle^{i}}{\partial x_2}\bigg|_{\phi=1} \tag{24}$$

Table 2
Average Nusselt numbers for $10^4 < Ra < 10^{10}$ with $\phi = 0.95$, $Da = K/H^2 = 0.2382 \times 10^{-5}$, $k_s/k_f = 1$ and $Pr = 1$

Model applied\Ra	10^4	10^6	10^8	10^{10}
Laminar solution	1.0000	1.2385	2.0230	2.7200
Turbulent solution	1.0000	1.2386	2.0231	2.7223

where β_i in Eq. (18) is a coefficient that expresses a jump condition in the shear stress at the interface. The interface conditions for k and ε, Eqs. (19)–(22), were proposed by [47], assuming continuity of k and ε, and their respective diffusive fluxes at the interface.

7. Numerical method and solution procedure

The numerical method employed for discretizing the governing equations is the control-volume approach. The flux blended deferred correction which combines linearly the Upwind Differencing Scheme (UDS) and Central Differencing Scheme (CDS), was used for interpolating the convective fluxes. The well-established SIMPLE algorithm [48] is followed for handling the pressure–velocity coupling. Individual algebraic equation sets were solved by the SIP procedure of [49]. Details on the validation of the numerical tool here employed can be found in previous publications, which include buoyant flows in hybrid (clear/porous) square cavities [50] and in different geometries, such as cylindrical annulus [36]. In those papers, as well as in [34–37], care was taken in order to check the solution against available numerical and experimental data in the literature.

8. Results and discussion

Calculations were performed for all cases using a 112×112 stretched grid with several points inside the boundary layers, as shown in Fig. 1b. Further, stretching of the grid aimed at resolving the flow structure inside the boundary layers by concentrating nodes close to external walls and about internal interfaces. The percent difference for the average Nusselt number on the heated wall calculated with larger grids was less than 1%. For this reason, all computations herein used the 112×112 stretched mesh. All cases simulated herein are compiled in Table 1.

Fig. 2 shows the isotherms and streamlines of a composite square cavity for Ra number ranging from 10^4 to 10^{10} with $\phi = 0.95$, $Da = 0.2382 \times 10^{-5}$, $k_s/k_f = 1$, $Pr = 1$. For the sake of simplicity, all calculations were performed with $K_{disp} = 0$ in Eq. (24).

For $Ra = 10^4$, the streamlines, form a single vortex confined only in the left of the clear region and the flow circulation in the porous medium is almost none (Fig. 2a). The isotherms are almost parallel to the heated wall indicating that the main mechanism of heat transfer is conduction (Fig. 2b). Increasing the Ra number to 10^6, the isotherms in the clear region starts to be distorted due to the increasing of the natural convection. However, in the porous region, the main mechanism of heat transfer is still conduction (Fig. 2d). The streamlines are now stronger than those for $Ra = 10^4$, but the flow structure still remains mainly in the clear region (Fig. 2c). Further increasing Ra to 10^8, the isotherms in the clear region are stratified and the convection mechanism is fully developed in such region. In the porous region, the isotherms become distorted due to the fluid that penetrates the porous layer inducing the also the natural convection (Fig. 2f). The fluid motion in the clear region is now very intense and the center of the single vortex is moved toward to the heated wall. In the porous region, the fluid starts to permeate the porous matrix inducing the natural convection in that region (Fig. 2e). Finally, for $Ra = 10^{10}$, the isotherms in both clear and porous region are stratified and the heat transfer in the solid region as a high temperature gradient (Fig. 2h). The fluid movement is stronger in both regions and the natural convection is also developed in the porous medium (Fig. 2g).

Fig. 3 also presents the effect of Ra on temperature field across the composite cavity. Upward velocities are presented in Fig. 3a at the cavity mid-height $y/H = 0.5$. For the sake of clarity, only a small portion of the solid layer is plotted at the right of Fig. 3a. For $Ra = 10^4$, convective currents exist only in the clear domain, and

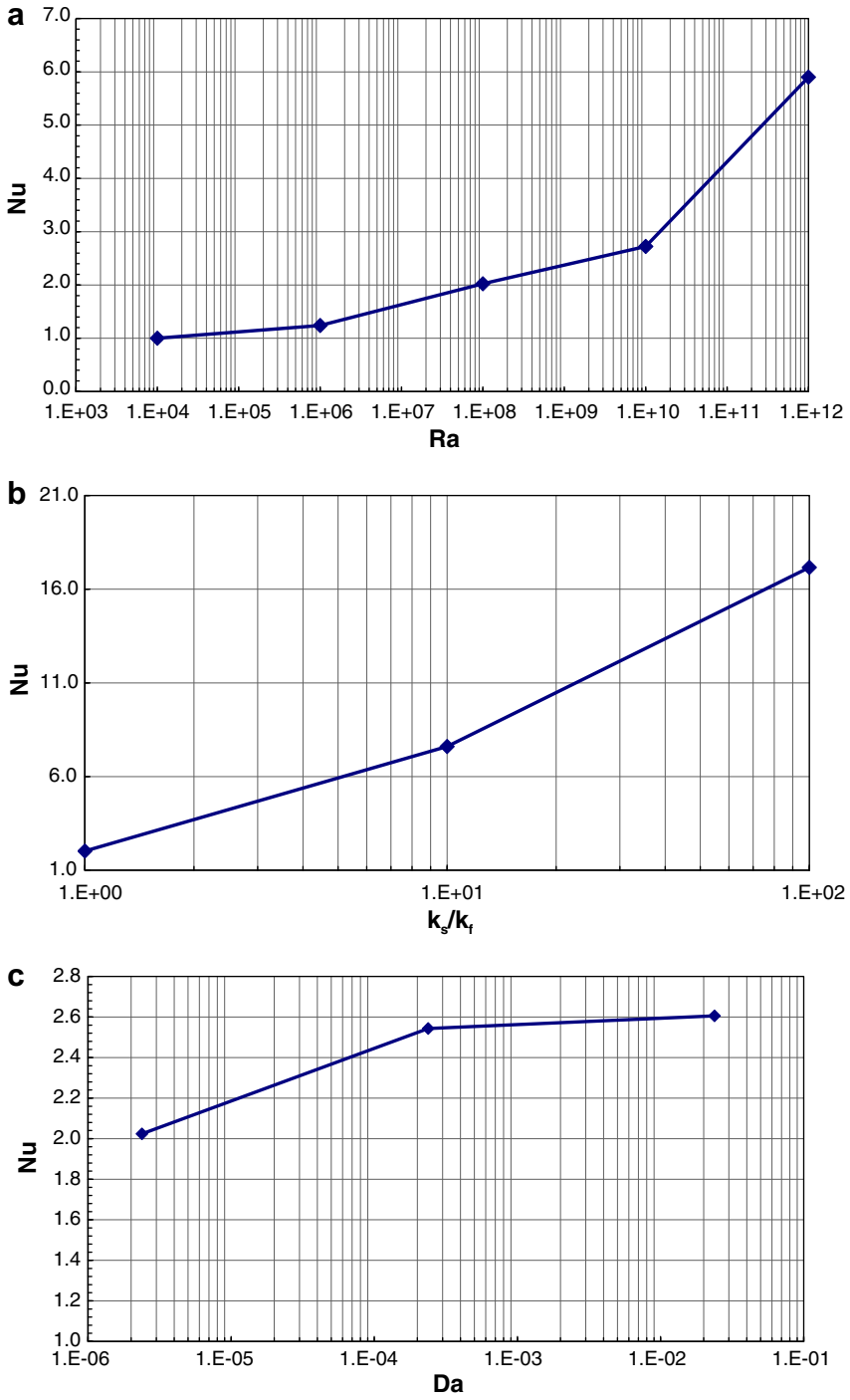

Fig. 6. Variation of cavity Nusselt number, *Nu*, as a function of: (a) *Ra*, (b) k_s/k_f, (c) *Da*.

a single recirculating bubble appears at the left of the unobstructed space, close to the hot wall. For $Ra = 10^6$, the recirculation regions grows filling the entire clear space. Further increasing *Ra* to 10^8, the flow enters the porous cavity in addition to recirculate in the clear region as well. With such *Ra*, boundary layers can be noticed at the interface porous-solid material as well as along the hot wall at the left. Finally, for $Ra = 10^{10}$, convective currents get stronger and a single large recirculation bubble fills both the porous and the clear domains. These observations corroborate those done earlier about Fig. 2.

In Fig. 3b corresponding temperature profiles at the same cavity height are plotted. The nearly conduction dominated regime for $Ra = 10^4$ stretches across the entire cavity, resulting in an almost linear temperature profile. Elongation of the recirculation bubble for $Ra = 10^6$ increases the temperature at the clear-porous interface, mixing the fluid within the clear regions. For higher values of *Ra*, the stratification regime covers not only the clear space but also the porous matrix. Thermal resistance across the cavity, for high *Ra* values, is concentrate in the solid material. Thermal control devices can then be engineered with appropriate layer material and dimensions in order to modulating heat transfer across such cavities.

Corresponding results for $\langle k \rangle^i$ as a function of *Ra* are presented in Fig. 4a, where dimensional values for the turbulent kinetic

energy, in $(m/s)^2$, are plotted across the cavity for $y/H = 0.5$. At $Ra = 10^4$, the weak recirculating bubble shown in Fig. 2a exists only in the clear domain and the levels of $\langle k \rangle^i$ are negligible everywhere in the cavity. For $Ra = 10^6$, the recirculation bubble grows and starts to penetrate the porous region (Fig. 2c), but its strength is not enough to generate turbulence. Only at $Ra = 10^{10}$ the strong currents ascending close to the hot wall and penetrating the porous region are able to generate turbulence (Fig. 2g), which is mostly confined within the boundary layers on the hot wall and attached to the solid material. Accordingly, as discussed in [30], the porous matrix contributes with the generation of turbulent kinetic energy via the extra term G^i in the $\langle k \rangle^i$ – Eq. (12). A corresponding two-dimensional map is shown in Fig. 4b, where $\langle k \rangle^i$ isolines for the left bottom part of the cavity are plotted ($x/H < 0.6$). Such two-dimensional view indicates the distribution of turbulence within the cavity, with higher values concentrated within the above-mentioned boundary layers.

The effect of changing the solid thermal conductivity values is shown next. Fig. 5b illustrates how temperature profiles are influenced when the thermal conductivity ratio k_s/k_f is varied from unity up to 100. For simplicity, the material of the solid is assumed to have the same thermal conductivity of that of the porous substrate. As such, only one unique value for k_s is adopted for both the porous and the solid material. One can observe that for the conditions in the figure and for $k_s/k_f = 1$, thermal resistance within the solid material is higher. As this ration increases ($k_s/k_f = 10$), heat is easily conducted though the solid and thermal resistance are equivalent in the two layers on the left of the cavity. For $k_s/k_f = 100$, either in the solid, due to high k_s, or within the stratified fluid layer at the left, due to stratification, thermal resistance is mostly confined within the porous layer. This result may indicate that such devices can be manufactured so that one can control where heat will encounter most resistance, which can be used to advantage when designing passive thermal control devices.

Fig. 5b indicates the effect of *Da* on temperature. For highly permeable materials, strong convective currents penetrate the porous substrate, causing a homogenization effect on the temperature in both the clear and within the porous layer. The figure also indicates that increasing *Da* past a certain value does not contribute to enhance heat transport across the cavity.

Table 2 shows the average Nusselt number in the heated wall for *Ra* ranging from 10^4 to 10^{10}. The table shows that for the range of *Ra* analyzed there are no significant variation between the laminar and turbulent model solution. Probably for higher values of *Ra*, remarkable variations between the two models might occur. Fig. 6 follows presenting the information on Table 2 in the form of graphics.

As mentioned, Fig. 6 consolidates results for the behavior of *Nu* as a function of distinct parameters here investigated, which were compiled in Table 2. First, Fig. 6a presents the increase of Nusselt as *Ra* is augmented, with corresponding *T* profiles given in Fig. 3b. Strong recirculating currents penetrating the porous material carry heat from hot wall at left to edge of the solid layer. Thermal resistance at high *Ra* is therefore sole controlled with the use of appropriate solid materials. Fig. 6b compiles *Nu* from the cases shown in Fig. 5a. Reducing the thermal resistance through the solid and fluid layer enhances the overall transfer of heat across the cavity, at least for the conditions here analyzed. Fig. 6c finally presents *Nu* for cases previously shown in Fig. 5b. As the porous matrix becomes more permeable, both the clear and the porous regions suffer stratification to a certain point, above which a further increase in *Da* does not enhances heat transfer, as can be seen by little variation on T profiles (Fig. 5b) and *Nu* values (Fig. 6c) for $Da > 2.38 \times 10^{-4}$.

Ultimately, results herein can help engineers in designing passive heat control systems by constructing composite walls made of layers of different materials and shapes.

9. Conclusions

This paper presented computations for laminar and turbulent flows with the macroscopic k–ε model with a wall function for natural convection in a square composite cavity. It is clearly seen from the figures that the fluid begins to permeate the porous medium for values of *Ra* greater than 10^6. At higher *Ra*, turbulent kinetic energy levels are higher along the hot wall and on the interface porous-solid media, as presented in Fig. 4. Nusselt numbers for a square composite cavity show that for the range of *Ra* analyzed there are no significant variation between the laminar and turbulent model solution. When comparing the effects of *Ra*, k_s/k_f and *Da* on *Nu*, results indicate that the solid phase properties have a greater influence in enhancing the overall heat transferred trough the cavity.

Ultimately, one can conclude that among the possibilities of using a different fluid (changing ν, α, β for varying *Ra*), a different solid material (k_s/k_f) or by changing the porous matrix shape (distinct K, $Da = K/H^2$), the use of a higher solid thermal conductivity can more efficiently enhance heat transfer across a cavity with a certain height H and subjected to a temperature difference ΔT.

Acknowledgment

The authors are thankful to CNPq and FAPESP, Brazil, for their financial support during the course of this research.

References

[1] D.A. Nield, A. Bejan, Convection in Porous Media, Springer, New York, 1992.
[2] D.B. Ingham, I. Pop, Transport Phenomena in Porous Media, Elsevier, Amsterdam, 1998.
[3] K.L. Walker, G.M. Homsy, Convection in porous cavity, J. Fluid Mech. 87 (1978) 449–474.
[4] A. Bejan, On the boundary layer regime in a vertical enclosure filled with a porous medium, Lett. Heat Mass Transfer 6 (1979) 93–102.
[5] V. Prasad, F.A. Kulacki, Convective heat transfer in a rectangular porous cavity-effect of aspect ratio on flow structure and heat transfer, J. Heat Transfer 106 (1984) 158–165.
[6] C. Beckermann, R. Viskanta, S. Ramadhyani, A numerical study of non-Darcian natural convection in a vertical enclosure filled with a porous medium, Num. Heat Transfer 10 (1986) 557–570.
[7] R.J. Gross, M.R. Bear, C.E. Hickox, The application of flux-corrected transport (Fct) to high Rayleigh number natural convection in a porous medium, in: Proceedings of the Eighth International Heat Transfer Conference, San Francisco, CA, 1986.
[8] D.M. Manole, J.L. Lage, Numerical Benchmark Results for Natural Convection in a Porous Medium Cavity, Heat and Mass Transfer in Porous Media, ASME Conference, Htd, vol. 216, 1992, pp. 55–60.
[9] A.C. Baytas, I. Pop, Free convection in oblique enclosures filled with a porous medium, Int. J. Heat Mass Transfer 42 (1999) 1047–1057.
[10] N. Massarotti, P. Nithiarasu, A. Carotenuto, Microscopic and macroscopic approach for natural convection in enclosures filled with fluid saturated porous medium, Int. J. Numer. Meth. Heat Fluid Flow 13 (7) (2003) 862–886.
[11] P. Nithiarasu, K. Ravindran, A new semi-implicit time stepping procedure for buoyancy driven flow in saturated porous medium, Comp. Meth. Appl. Mech. Eng. 165 (1998) 147–154.
[12] P. Nithiarasu, K.S. Sujatha, K. Ravindran, K.N. Seetharamu, T. Sundararajan, Non-Darcy natural convection in a hydrodynamically and thermally anisotropic porous medium, Comp. Meth. Appl. Mech. Eng. 188 (2000) 413–430.
[13] P. Nithiarasu, K.N. Seetharamu, T. Sundararajan, Double-diffusive natural convection in an enclosure filled with saturated porous medium a generalized non-Darcy approach, Numer. Heat Transfer Part A 30 (1996) 413–426.
[14] I.P. Jones, A comparison problem for numerical methods in fluid dynamics: the double-glazing problem, in: R.W. Lewis, K. Morgan (Eds.), Numerical Methods in Thermal Problems, Pineridge Press, Swansea, UK, 1979, pp. 338–348.
[15] G. de Vahl Davis, Natural convection in a square cavity: a benchmark numerical solution, Int. J. Numer. Methods Fluids 3 (1983) 249–264.
[16] G. de Vahl Davis, I.P. Jones, Natural convection in a square cavity – a comparison exercise, Int. J. Numer. Methods Fluids 3 (1983) 227–248.
[17] N.C. Markatos, K.A. Pericleous, Laminar and turbulent natural convection in an enclosed cavity, Int. J. Heat Mass Transfer 27 (1984) 755–772.
[18] H. Ozoe, A. Mouri, M. Ohmuro, S.W. Churchill, N. Lior, Numerical calculations of laminar and turbulent natural convection in water in rectangular channels heated and cooled isothermally on the opposing vertical walls, Int. J. Heat Mass Transfer 28 (1985) 125–138.

[19] R.A.W.M. Henkes, F.F. Van Der Vlugt, C.J. Hoogendoorn, Natural-convection flow in a square cavity calculated with low-Reynolds-number turbulence models, Int. J. Heat Mass Transfer 34 (2) (1991) 377–388.
[20] T. Fusegi, J.M. Hyun, K. Kuwahara, Three-dimensional simulations of natural convection in a sidewall-heated cube, Int. J. Numer. Methods Fluids 3 (1991) 857–867.
[21] G. Barakos, E. Mitsoulis, D. Assimacopoulos, Natural convection flow in a square cavity revised: laminar and turbulent models with wall function, Int. J. Numer. Methods Fluids 18 (1994) 695–719.
[22] T. Masuoka, Y. Takatsu, Turbulence model for flow through porous media, Int. J. Heat Mass Transfer 39 (13) (1996) 2803–2809.
[23] F. Kuwahara, A. Nakayama, H. Koyama, A numerical study of thermal dispersion in porous media, J. Heat Transfer 118 (1996) 756–761.
[24] F. Kuwahara, A. Nakayama, Numerical modeling of non-Darcy convective flow in a porous medium, in: Heat Transfer 1998: Proceedings of 11th International Heat Transfer Conference, Kyongyu, Korea, Taylor & Francis, Washington, DC, vol. 4, 1998, pp. 411–416.
[25] A. Nakayama, F. Kuwahara, A macroscopic turbulence model for flow in a porous medium, J. Fluids Eng. 121 (1999) 427–433.
[26] K. Lee, J.R. Howell, Forced convective and radiative transfer within a highly porous layer exposed to a turbulent external flow field, in: Proceedings of the 1987 ASME-JSME Thermal Engineering Joint Conference, Honolulu, Hawaii, ASME, New York, NY, vol. 2, 1987, pp. 377–386.
[27] B.V. Antohe, J.L. Lage, A general two-equation macroscopic turbulence model for incompressible flow in porous media, Int. J. Heat Mass Transfer 40 (13) (1997) 3013–3024.
[28] D. Getachewa, W.J. Minkowycz, J.L. Lage, A modified form of the k–ε model for turbulent flow of an incompressible fluid in porous media, Int. J. Heat Mass Transfer 43 (2000) 2909–2915.
[29] M.H.J. Pedras, M.J.S. de Lemos, Computation of turbulent flow in porous media using a low-Reynolds k–ε model and an infinite array of transversally displaced elliptic rods, Numer. Heat Transfer Part A Appl. 43 (6) (2003) 585–602.
[30] M.J.S. de Lemos, Turbulence in Porous Media: Modeling and Applications, Elsevier, Amsterdam, 2006.
[31] F.D. Rocamora Jr., M.J.S. de Lemos, Analysis of convective heat transfer of turbulent flow in saturated porous media, Int. Commun. Heat Mass Transfer 27 (6) (2000) 825–834.
[32] M.J.S. de Lemos, F.D. Rocamora, Turbulent transport modeling for heated flow in rigid porous media, in: Proceedings of the 12th International Heat Transfer Conference, Grenoble, France, August 18–23, 2002, pp. 791–795.
[33] M.J.S. de Lemos, E.J. Braga, Modeling of turbulent natural convection in saturated rigid porous media, Int. Commun. Heat Mass Transfer 30 (5) (2003) 615–624.
[34] E.J. Braga, M.J.S. de Lemos, Turbulent natural convection in a porous square cavity computed with a macroscopic k–ε model, Int. J. Heat Mass Transfer 47 (2004) 5639–5650.
[35] E.J. Braga, M.J.S. de Lemos, Heat transfer in enclosures having a fixed amount of solid material simulated with heterogeneous and homogeneous models, Int. J. Heat Mass Transfer 48 (23–24) (2005) 4748–4765.
[36] E.J. Braga, M.J.S. de Lemos, Simulation of turbulent natural convection in a porous cylindrical annulus using a macroscopic two-equation model, Int. J. Heat Mass Transfer 49 (23–24) (2006) 4340–4351.
[37] E.J. Braga, M.J. S de Lemos, Computation of turbulent free convection in left and right tilted porous enclosures using a macroscopic k–ε model, Int. J. Heat Mass Transfer 51 (21–22) (2008) 5279–5287.
[38] M.J.S. de Lemos, M.S. Mesquita, Turbulent mass transport in saturated rigid porous media, Int. Commun. Heat Mass Transfer 30 (1) (2003) 105–113.
[39] M.B. Saito, M.J.S. de Lemos, Interfacial heat transfer coefficient for non-equilibrium convective transport in porous media, Int. Commun. Heat Mass Transfer 32 (5) (2005) 667–677.
[40] M.B. Saito, M.J.S. de Lemos, A correlation for interfacial heat transfer coefficient for turbulent flow over an array of square rods, J. Heat Transfer 128 (2006) 444–452.
[41] M.J.S. de Lemos, L.A. Tofaneli, Modeling of double-diffusive turbulent natural convection in porous media, Int. J. Heat Mass Transfer 47 (19–20) (2004) 4221–4231.
[42] M.J.S. de Lemos, Turbulent kinetic energy distribution across the interface between a porous medium and a clear region, Int. Commun. Heat Mass Transfer 32 (1–2) (2005) 107–115.
[43] M.J.S. de Lemos, R.A. Silva, Turbulent flow over a layer of a highly permeable medium simulated with a diffusion-jump model for the interface, Int. J. Heat Mass Transfer 49 (3–4) (2006) 546–556.
[44] F. Kuwahara, Y. Kameyama, S. Yamashita, A. Nakayama, Numerical modeling of turbulent flow in porous media using a spatially periodic array, J. Porous Media 1 (1) (1998) 47–55.
[45] S. Ergun, Fluid flow through packed columns, Chem. Eng. Pro. 48 (2) (1952) 89–94.
[46] J.A. Ochoa-Tapia, S. Whitaker, Momentum transfer at the boundary between a porous medium and a homogeneous fluid – I. Theoretical development, Int. J. Heat Mass Transfer 38 (1995) 2635–2646.
[47] K. Lee, J.R. Howell, Forced convective and radiative transfer within a highly porous layer exposed to a turbulent external flow field, in: Proceedings of the 1987 ASME-JSME Thermal Engineering Joint Conference, vol. 2, 1987, pp. 377–386.
[48] S.V. Patankar, D.B. Spalding, A calculation procedure for heat, mass and momentum transfer in three-dimensional parabolic flows, Int. J. Heat Mass Transfer 15 (1972) 1787.
[49] H.L. Stone, Iterative solution of implicit approximations of multi-dimensional partial differential equations, SIAM J. Num. Anal. 5 (1968) 530–558.
[50] E.J. Braga, M.J.S. de Lemos, Turbulent heat transfer in an enclosure with a horizontal porous plate in the middle, J. Heat Transfer 128 (11) (2006) 1122–1129.